Decrease of $Ca_3Co_4O_{9+\delta}$ thermal conductivity by Yb-doping

G. Klirat[1], M. A. Aksan[1], Sh. Rasekh[2], M. A. Madre[2,*], J. C. Diez[2], A. Sotelo[2]

[1] Inonu Universitesi, Fen Edebiyat Fakultesi, Fizik Bolumu, 44280 Malatya, TURKEY
[2] ICMA (CSIC-Universidad de Zaragoza), Maria de Luna, 3. 50018 Zaragoza, SPAIN

Abstract

In this study, the effect of Yb-substitution on the structural, electrical and thermal transport properties of the $Ca_3Co_4O_{9+\delta}$ system has been investigated at low temperature region (between 10 and 300 K). The resistivity of samples increases with increasing the Yb-concentration in the system. All the samples show a metal-semiconductor transition below 85 K. In the analysis based on *Strongly Correlated Fermi Liquid Model*, an increased bandwidth and a reduced electronic correlation are found. It has also been found that the energy gap, E_0, value also decreases with Yb-substitution. The samples show positive thermoelectric power, indicating that dominant charge carriers are holes in all the samples. The thermoelectric power value decreases with Yb-substitution. From Mott equation, it is determined that the Fermi energy and hole concentration decrease in the Yb-susbtituted samples, compared to the undoped ones. Thermal conductivity, κ, is decreased in about 50 % of the measured in undoped samples for the 0.01 and 0.03 Yb-doped samples at 300 K. Highest figure of merit, ZT, value is found to be 5.4 10^{-3} at 300 K for the unsubstituted sample and the ZT value decreases by the substitution.

Keywords: ceramics; doping; electrical transport; thermal conductivity

Corresponding author: M. A. Madre
e-mail: amadre@unizar.es
Address: ICMA (CSIC-Universidad de Zaragoza), Maria de Luna, 3. 50018 Zaragoza, SPAIN
Tel: +34 976762617
Fax: +34 976761957

Introduction

Thermoelectric (TE) materials for practical electric power generation systems should possess high energy conversion efficiency. TE energy conversion has important advantages to be used to transform solar energy into electricity at lower cost than photovoltaic energy [1]. The TE materials conversion efficiency is quantified by the dimensionless figure of merit ZT, defined as $S^2T/\rho\kappa$, where S is the thermoelectric power, ρ electrical resistivity, κ thermal conductivity, and T is absolute temperature [2]. From this expression, it is clear that a TE material for practical applications must involve high thermoelectric power and low electrical resistivity, with low thermal conductivity and high working temperatures.

The discovery of large S values in Na_xCoO_2 [3], with high ZT at 300 K, has opened a new research field. From this discovery, great efforts have been made to explore new ceramic families with high thermoelectric performances. In the last years, many studies have been performed in other layered cobaltites, such as $[Ca_2CoO_3][CoO_2]_{1.62}$, $[Bi_{0.87}SrO_2]_2[CoO_2]_{1.82}$ and $[Bi_2Ca_2O_4][CoO_2]_{1.65}$ which also exhibit attractive thermoelectric properties [4-6]. In these systems, the crystal structure is formed by two different layers, showing an alternate stacking of a common conductive CdI_2-type CoO_2 layer with a two-dimensional triangular lattice and a block layer, composed of insulating rock-salt-type (RS) layers. Both sublattices (RS and CdI_2-type layers) possess common *a*- and *c*-axis lattice parameters and β angles but different *b*-axis length, causing a misfit along the *b*-direction [7,8].

One of the main factors affecting the thermoelectric performances of this kind of materials is the electrical resistivity which should be maintained as low as possible to avoid Joule heating. The resistivity values in ceramic materials are influenced by a number of different parameters as content and distribution of secondary phases, porosity, oxygen content, etc. As a consequence, many different synthesis methods have been used in order to prepare thermoelectric and other layered ceramic materials [4,9-12]. On the other hand, layered cobaltites are materials with a strong crystallographic anisotropy; therefore the alignment of plate-like grains by mechanical and/or chemical processes has been studied to attain macroscopic properties comparable to those obtained on single crystals mainly due to the decrease of their electrical resistivity. Some techniques have been shown to be adequate to obtain a good grain orientation in several oxide ceramic systems, such as templated grain

growth (TGG) [8], hot pressing [13], spark plasma sintering (SPS) [14], laser floating zone [15] or electrically assisted laser floating zone [16]. Other possibilities arising from their crystallographic structure are the cationic substitutions in the RS layer, which can modify the misfit relationship. From this point of view, it is clear that these substitutions can modify the thermoelectric performances, as it is reported for substitutions of B [17] or Sb [18] for Ca in $[Ca_2CoO_3][CoO_2]_{1.62}$, Pb for Bi [19] or Sr by Ca [20] in $[Bi_2Ca_2O_4][CoO_2]_{1.65}$.

The aim of this work is studying the effect produced by the substitution of small amounts of Yb for Ca on the microstructure and thermoelectric characteristics of $Ca_3Co_4O_{9+\delta}$ ceramic materials.

Experimental

The initial $Ca_{3-x}Yb_xCo_4O_{9+\delta}$ (x = 0.00, 0.01, 0.03, and 0.05) polycrystalline ceramics were prepared from commercial $CaCO_3$ (> 98.5 %, Panreac), Co_3O_4 (99.7 %, Alfa Aesar), and Yb_2O_3 (99.9 %, Aldrich) powders by the classical solid state method. The powders were weighed in the appropriate proportions, well mixed and ball milled for 30 minutes at 300 rpm, in acetone media, in a planetary agate ball mill. The obtained slurry has been heated in a rapid evaporation system equipped with infrared radiation until the acetone has been totally evaporated. The dry mixture was then manually milled in order to avoid the presence of the agglomerates in the next steps and, as a consequence, favouring the alkaline earth carbonates decomposition. After milling, the fine powdered mixture has been thermally treated, in a two steps process, at 750 ºC and 800 ºC for 12 h under air, with an intermediate manual milling. The objective of this thermal treatment is assuring the total decomposition of calcium carbonates, as reported previously [21], which improve the mixture reactivity in the sintering processes. After the thermal treatments, the powders were milled again and uniaxially pressed at 400 MPa for 1 minute in order to obtain green ceramic parallelepipeds (approximately 3 mm x 2.5 mm x 14 mm), with an adequate size for their thermoelectric characterization. The green ceramics were subsequently sintered in the optimal conditions found in previous works with the help of the CaO-CoO phase diagram [22], and consisting in one step heating at 900 ºC for 24 h with a final furnace cooling which are the best determined conditions to produce the $Ca_3Co_4O_{9+\delta}$ phase [23].

Powder X-ray diffraction (XRD) patterns have been systematically recorded in order to identify the different phases in the thermoelectric sintered materials. Data have been collected at room temperature, with 2θ ranging between 5 and 40 degrees, using a Rigaku D/max-B X-ray powder diffractometer working with Cu K_α radiation. Microstructural investigations were performed using a Field Emission Scanning Electron Microscope (FESEM, Carl Zeiss Merlin) fitted with an energy dispersive spectrometry (EDS) analyzer.

Temperature dependence of resistivity (ρ−T), thermoelectric power (*S*–T) and thermal conductivity (κ–T) of the samples were measured simultaneously with 9 Tesla Quantum Design physical properties measurement system (PPMS) between 10 and 300 K. *S* was determined by dividing the voltage difference (ΔV) to the temperature gradient (ΔT) between the two ends of the sample (S=ΔV/ΔT). Thermal conductivity measurements were carried out using the steady-state method.

Results and discussion

The XRD patterns for the $Ca_{3-x}Yb_xCo_4O_{9+\delta}$ samples are shown in Fig. 1. It is obvious that all the samples have very similar diffraction patterns. All the materials mainly consist of the thermoelectric $Ca_3Co_4O_{9+\delta}$ phase with monoclinic symmetry [24] which is in agreement with previously reported data [25]. However, a small amount of secondary phase, $Ca_3Co_2O_6$, (marked with * and situated at ~ 31º) is also obtained [25,26]. It should be mentioned that the peak indicated with • corresponds to the (111) diffraction plane of Si used as internal reference.

Fig. 2 shows SEM micrographs performed on the surface of the samples. It can be clearly seen that all samples are composed by randomly oriented plate-like grains with a relatively broad grain sizes distribution, which is a typical $Ca_3Co_4O_{9+\delta}$ formation when they are prepared by the solid state sintering process. It has been found that the samples show a relatively high degree of porosity and major phase is the thermoelectric $Ca_3Co_4O_{9+\delta}$ one (grey contrast, denoted by #1) which can be observed as well defined plate-like grains. Secondary phase $Ca_3Co_2O_6$ (denoted by #2, slightly darker grey contrast) is also seen in the highly substituted samples (≥ 0.03 Yb content). These results are in good agreement with the XRD results. On the other hand, microstructural observation has shown that in the highest substituted sample new small grains appear (denoted by #3). EDS analysis has shown a cation

relationship Ca:Yb:Co of 0.7:2:1. From the formation of these Yb-based secondary phases it can be deduced that the nominal 0.05 Yb addition cannot be incorporated in the $Ca_3Co_4O_{9+\delta}$ crystal structure. As a consequence, it can be inferred that this Yb amount is higher its the maximum solubility in the $Ca_3Co_4O_{9+\delta}$ phase.

Fig. 3 shows the temperature dependence of the resistivity of the $Ca_{3-x}Yb_xCo_4O_{9+\delta}$ system. The resistivity increases with increasing the Yb-concentration in the system. Extra electrons are introduced by substitution of Yb^{3+} for Ca^{2+} in the $Ca_3Co_4O_{9+\delta}$ system, so hole concentration decreases in the system, compared to the unsubstituted sample, Table I. Decrease of the hole concentration in the system leads to the increase of the resistivity. It is believed that the increase in the amount of the porosity and so weak-link among the grains in the Yb-substituted samples causes the increase in the resistivity and impairs the electrical transport properties of the samples.

In all the samples, the electrical resistivity decreases with increasing temperature, indicating a typical characteristic of semiconducting behavior and then increased slowly with increasing temperature, indicating a typical characteristic of metallic one. Transition temperature (T_{IM}) from semiconducting to metallic shifts to lower temperatures with increasing the Yb-substitution level. It is believed that this type of transition in $Ca_3Co_4O_{9+\delta}$ may arise from the incommensurate spin-density-wave (IC-SDW) state [27-29]. In IC-SDW state, the charge carriers will be localized, which leads to semiconducting state. This is manifested as a broadband below 80 K in the ρ-T curve. Similar results have also been obtained in the studies reported by some researchers [30,31].

Strongly correlated Fermi liquid behavior between T_{IM} and T* exists in $Ca_3Co_4O_{9+\delta}$ system, in which T* is defined by the transition temperature from Fermi liquid to incoherent metal. In strongly correlated Fermi liquid region between TIM and T*, the resistivity data can be described as:

$$\rho=\rho_A+AT^2 \qquad (1)$$

where A is the Fermi liquid transport coefficient, ρ_A is the residual resistivity due to the domain boundaries and other temperature dependent scattering mechanisms, AT^2 implies the electron–electron scattering mechanism of carriers. According to the

dynamical mean field theory (DMFT) [32], T*~ 1/m* and A ~ $(m^*)^2$ for a Fermi liquid. We have fitted the resistivity data to equation (1) and displayed the results in Fig. 4. It is seen that the ρ(T) is well fitted to Equation (1). T* is defined as the deviation temperature from the linear dependence in Fig. 4. The obtained T* values are listed in Table I. It can be concluded that the T* value increases by the Yb-substitution level instead of the x=0.01 Yb-substitution level (see Fig. 4), indicating that the temperature region of electron–electron scattering becomes wider [30]. Increase in T* suggests the decrease of m* which indicates an increased bandwidth and a reduced electronic correlation.

In the IC-SDW region, the variation of the $\rho(T)$ obeys thermally activated behavior explained by the formula:

$$\frac{1}{\rho} = \mu(T) exp\left(-\frac{E_0}{k_B T}\right) \qquad (2)$$

where $\mu(T)$ is the mobility of carriers, and E_0 the energy gap caused by the SDW at Fermi surface [30,33,34]. The $\rho(T)$ data in the IC-SDW region are fitted to equation (2), and the results are plotted in Fig. 5 and inset. The fitting parameters are presented in Table I. It is found that the energy gap, E_0, value decreases by the Yb-substitution. This clearly indicates that the Yb-substitution has a negative effect on the formation of the IC-SDW, it becomes more unstable and the localization of carriers weakens by Yb-substitution.

The temperature dependence of thermoelectric power of the $Ca_{3-x}Yb_xCo_4O_{9+\delta}$ system is shown in Fig. 6. All the samples show positive thermoelectric power over the whole measured temperature range, indicating that dominant charge carriers are holes. The *S* value decreases for the x=0.01 and x=0.03 Yb-substituted samples and then increases for the x=0.05 Yb-substituted ones. In general, the decrease of carrier concentration in these materials should increase the electrical resistivity and so the thermoelectric power. However, in the present study, *S* decreases by the Yb-substitution at low temperatures. We believe that the deterioration of electronic correlation plays more important role than the decrease of the carrier concentration on thermoelectric power behavior of the samples.

S for the hole type conduction can be analyzed by the modified Mott formula:

$$S = \frac{c_e}{n} + \frac{\pi^2 k_B^2 T}{3e}\left[\frac{\partial \ln \mu(\varepsilon)}{\partial \varepsilon}\right]_{\varepsilon=\varepsilon_F} \quad (3)$$

where n is carrier concentration, $\mu(\varepsilon)$ the energy correlated carrier mobility, C_e the specific heat, and k_B Boltzmann constant. If S is inversely proportional to n, the first term is dominant in equation (3). Otherwise, if the second term is dominant, S is associated with the electronic structure [31,34]. Taking into account the data obtained in these samples, it can be deduced that the second condition is valid in the present study.

Assuming that the mobility or conductivity is proportional to the energy and there is a T-independent mean free path and T-independent relaxation for carriers, equation (3) becomes

$$S_d(T) = \frac{\pi^2 k_B^2 T}{3eE_F} \quad (4)$$

where E_F is the Fermi energy. E_F and n values obtained using equation (4) are shown in Table I. The Fermi energy values are in good agreement with the values found from band structure calculations [35-37]. However, the E_F and n values decrease in the Yb-susbtituted samples, compared to the unsubstituted ones. More electrons will be introduced in the system producing the decrease of hole concentration by the substitution of trivalent Yb^{3+} for Ca^{2+} in the system, which cause the decrease of the carrier concentration in these materials and so E_F.

Fig. 7 shows the temperature dependence of thermal conductivity κ of the $Ca_{3-x}Yb_xCo_4O_{9+\delta}$ system. Similar $\kappa(T)$ trend is obtained for all the samples. It is found that the magnitude of κ decreases with increasing the Yb-content in the $Ca_3Co_4O_{9+\delta}$ system. It is thought that the predominant contribution to κ comes from the phonon thermal conductivity, κ_{ph}. The impurities and defects formed by the Yb-substitution induce non-harmonic phonon vibration in the materials. Thus, scattering of phonons from the impurities and defects shortens the mean free path of the phonons and causes a strong decrease in κ_{ph}. So, total thermal conductivity, κ, decreases with an increasing substitution level. The highest decrease is produced with the 0.01 and

0.03 Yb substitution which is around 50 % lower than the obtained in the undoped samples at 300 K.

Fig. 8 shows the figure of merit ($ZT=S^2T/\rho\kappa$) versus temperature curves of the $Ca_{3-x}Yb_xCo_4O_{9+\delta}$ system. The ZT values of the samples are presented in Table I. Highest ZT value is found to be 5.4 10^{-3} at 300 K for the unsubstituted samples. It is seen that the ZT value decreases by the substitution. However, the ZT value of the samples tends to increase with temperature.

In spite of the ZT decrease with Yb-doping, it is important to highlight the great decrease of thermal conductivity. As a consequence, its combination with other substituting elements which raise thermoelectric power and/or electrical resistivity could lead to an important raise of ZT, approaching this material to practical applications.

Conclusions

In the present study, the effect of the Yb-substitution on the structural, electrical and thermal transport properties in the $Ca_3Co_4O_{9+\delta}$ system has been investigated. The structural analysis reveals that the main phase is $Ca_3Co_4O_{9+\delta}$ with some secondary phases. Especially, in the case of the highest doped samples, Yb-rich phases are identified in microstructural studies. The resistivity of the samples shows a metal-semiconductor transition below 85 K, which is attributed to IC-SDW state. The resistivity increases with the Yb-content in the system. Moreover, the temperature dependence of resistivity of the samples indicates a reduction in the electronic correlation in the Yb-substituted samples. The thermoelectric power decreases by Yb-substitution which is associated with the deterioration of electronic correlation of the samples. It is determined that the magnitude of thermoelectric power, κ, decreases with increasing the Yb-content. In conjunction with the other results, it is believed that the dominant contribution to κ comes from the phonon thermal conductivity, κ_{ph}. Highest ZT value is found to be 5.4 10^{-3} at 300 K for the unsubstituted samples. These results clearly show the great benefits provided by Yb in the decrease of thermal conductivity. As a consequence, its combination with other substituting elements which raise thermoelectric power and/or electrical resistivity

could lead to an important raise of ZT, approaching this material to practical applications.

Acknowledgements

The authors wish to thank the MINECO-FEDER (Project MAT2013--46505-C3-1-R) and the Gobierno de Aragón and Fondo Social Europeo (Research Groups T12 and T87) for financial support. The technical contributions of C. Estepa and C. Gallego are also acknowledged.

References

1. W. Liu, X. Yan, G. Chen, Z. Ren, Recent advances in thermoelectric nanocomposites, Nano Energy 1, 42-56 (2012).

2. D.M. Rowe, in: D.M. Rowe (Ed.), Thermoelectrics Handbook: Macro to Nano, 1st edn, CRC Press, Boca Raton, FL, 2006, pp. 1-3–1-7.

3. I. Terasaki, Y. Sasago, K. Uchinokura, Large thermoelectric power in NaCo2O4 single crystals, Phys. Rev. B 56, 12685–12687 (1997).

4. A. Sotelo, G. Constantinescu, Sh. Rasekh, M.A. Torres, J.C. Diez, M.A. Madre, Improvement of thermoelectric properties of $Ca_3Co_4O_9$ using soft chemistry synthetic methods, J. Eur. Ceram. Soc. 32, 2415-2422 (2012).

5. J.C. Diez, E. Guilmeau, M.A. Madre, S. Marinel, S. Lemmonier, A. Sotelo, Improvement of $Bi_2Sr_2Co_{1.8}O_x$ thermoelectric properties by laser floating zone texturing, Solid State Ionics 180, 827-830 (2009).

6. W. Kobayashi, S. Hebert, H. Muguerra, D. Grebille, D. Pelloquin, A. Maignan, Thermoelectric properties in the misfit-layered-cobalt oxides $[Bi_2A_2O_4]$ $[CoO_2]_{b1/b2}$ (A=Ca, Sr, Ba, b(1)/b(2)=1.65, 1.82, 1.98) single crystals. In I. Kim (Ed.), Proceedings ICT 07: Twenty-sixth international conference on hermoelectric, Korea. 2008. pp. 117-120.

7. A. Maignan, S. Hebert, M. Hervieu, C. Michel, D. Pelloquin, D. Khomskii, Magnetoresistance and magnetothermopower properties of Bi/Ca/Co/O and Bi(Pb)/Ca/Co/O misfit layer cobaltites. J. Phys.: Condens. Matter 15, 2711–2723 (2003).

8. H. Itahara, C. Xia, J. Sugiyama, T. Tani, Fabrication of textured thermoelectric layered cobaltites with various rock salt-type layers by using b-$Co(OH)_2$ platelets as reactive templates, J. Mater. Chem. 14, 61–66 (2004).

9. A. Sotelo, Sh. Rasekh, M.A. Madre, E. Guilmeau, S. Marinel, J.C. Diez, Solution-based synthesis routes to thermoelectric $Bi_2Ca_2Co_{1.7}O_x$, J. Eur. Ceram. Soc. 31, 1763-1769 (2011).

10. C.S. Sanmathi, Y. Takahashi, D. Sawaki, Y. Klein, R. Retoux, I. Terasaki, J. G. Noudem, Microstructure control on thermoelectric properties of $Ca_{0.96}Sm_{0.04}MnO_3$ synthesised by co-precipitation technique, Mater. Res. Bull. 45, 558-563 (2010).

11. A. Sotelo, Sh. Rasekh, M.A. Torres, P. Bosque, M.A. Madre, J.C. Diez, Effect of synthesis methods on the $Ca_3Co_4O_9$ thermoelectric ceramic performances, J. Solid State Chem. 221, 247-254 (2015)

12. N.Y. Wu, T.C. Holgate, N.V. Nong, N. Pryds, S. Linderoth, High temperature thermoelectric properties of $Ca_3Co_4O_{9+\delta}$ by auto-combustion synthesis and spark plasma sintering, J. Eur. Ceram. Soc. 34, 925-931 (2014)
13. H. Wang, X. Sun, X. Yan, D. Huo, X. Li, J.-G. Li, X. Ding, Fabrication and thermoelectric properties of highly textured $Ca_9Co_{12}O_{28}$ ceramic, J. Alloys Compds. 582, 294-298 (2014).
14. H.-Q. Liu, F.-P. Wang, F. Liu, Y. Song, Z.-H. Jiang, Thermoelectric performance of SPS sintered $[(Ca_{0.95}M_{0.05})_2CoO_3][CoO_2]_{1.61}$, J. Mater. Sci.: Mater. Electron. 17 (7), 525-528 (2006).
15. J.C. Diez, Sh. Rasekh, M.A. Madre, E. Guilmeau, S. Marinel, A. Sotelo, Improved Thermoelectric Properties of Bi-M-Co-O (M = Sr, Ca) Misfit Compounds by Laser Directional Solidification, J. Electron. Mater. 39, 1601-1605 (2010)
16. N.M. Ferreira, Sh. Rasekh, F.M. Costa, M.A. Madre, A. Sotelo, J.C. Diez, M.A. Torres, New method to improve the grain alignment and performance of thermoelectric ceramics, Mater. Lett. 83, 144-147 (2012).
17. S. Demirel, S. Altin, M.A. Aksan, High temperature thermoelectric properties of the $Ca_{3-x}B_xCo_4O_9$ system, J. Mater. Sci.: Mater. Electron. 24, 4406-4410 (2013).
18. S. Demirel, M.A. Aksan, S. Altin, Low temperature electrical and thermal transport properties of the $Ca_{3-x}Sb_xCo_4O_9$ system, J. Mater. Sci.: Mater. Electron. 23, 2251-2256 (2012).
19. A. Sotelo, Sh. Rasekh, E. Guilmeau, M.A. Madre, M.A. Torres, S. Marinel, J.C. Diez, Improved thermoelectric properties in directionally grown $Bi_2Sr_2Co_{1.8}O_y$ ceramics by Pb for Bi substitution, Mater. Res. Bull. 46, 2537-2542 (2011).
20. N. Sun, S.T. Dong, B.B. Zhang, Y.B. Chen, J. Zhou, S.T. Zhang, Z.B. Gu, S.H. Yao, Y.F. Chen, Intrinsically modified thermoelectric performance of alkaline-earth isovalently substituted $[Bi_2AE_2O_4][CoO_2]_y$ single crystals, J. Appl. Phys. 114, 043705 (2013).
21. M.A. Madre, F.M. Costa, N.M. Ferreira, A. Sotelo, M.A. Torres, G. Constantinescu, Sh. Rasekh, J.C. Diez, Preparation of high-performance $Ca_3Co_4O_9$ thermoelectric ceramics produced by a new two-step method, J. Eur. Ceram. Soc. 33, 1747-1754 (2013)
22. D. Sedmidubsky, V. Jakes, O. Jankovsky, J. Leitner, Z. Sofer, J. Hejtmanek, Phase equilibria in Ca-Co-O system, J. Solid State Chem. 194, 199-205 (2012).

23. J.C. Diez, M.A. Torres, Sh. Rasekh, G. Constantinescu, M.A. Madre, A. Sotelo, Enhancement of $Ca_3Co_4O_9$ thermoelectric properties by Cr for Co substitution, Ceram. Int. 39, 6051-6056 (2013).
24. A.C. Masset, C. Michel, A. Maignan, M. Hervieu, O. Toulemonde, F. Studer, B. Raveau, Misfit-layered cobaltite with an anisotropic giant magnetoresistance: $Ca_3Co_4O_9$, Phys. Rev. B, 62, 166-175 (2000).
25. E. Woermann, A. Muan, Phase equilibria in the system CaO-cobalt oxide in air. J. Inorg. Nucl. Chem. 32, 1455-1459 (1970).
26. Y.C. Liou, W.C. Tsai, W.Y. Lin, U.R. Lee, Synthesis of $Ca_3Co_4O_9$ and $CuAlO_2$ ceramics of the thermoelectric application using a reaction-sintering process, J. Aust. Ceram. Soc. 44, 17–22 (2008).
27. A. Bhaskar, Z.R. Lin, C.-J. Liu, Thermoelectric and magnetic properties of $Ca_3Co_{4-x}Cu_xO_{9+\delta}$ with x = 0.00, 0.05, 0.07, 0.10 and 0.15, Mater. Res. Bull. 48, 4884–4888 (2013).
28. J. Sugiyama, H. Itahara, T. Tani, J.H. Brewer, E.J. Ansaldo, Magnetism of layered cobalt oxides investigated by muon spin rotation and relaxation, Phys. Rev. B 66, 134413 (2002).
29. J. Sugiyama, J.H. Brewer, E.J. Ansaldo, H. Itahara, K. Dohmae, Y. Seno, C. Xia, T. Tani, Hidden magnetic transitions in the thermoelectric layered cobaltite $[Ca_2CoO_3]_{0.62}[CoO_2]$, Phys. Rev. B 68, 134423 (2003).
30. D. Dai, B. Zhao, Y. Huang, Y. Sun, A. Xie, Y. Shen, Suppressed spin-density-wave transition and enhanced electrical conductivity in chlorine doped $Ca_3Co_4O_{9-x}Cl_x$ ceramics, J. Alloys Compnd. 556, 228–233 (2013).
31. Y. Wang, Y. Sui, P. Ren, L. Wang, X. Wang, W. Su, H. Fan, Strongly correlated properties and enhanced thermoelectric response in $Ca_3Co_{4-x}M_xO_{9+\delta}$ (M=Fe, Mn and Cu), Chem. Mater. 22, 1155–1163 (2010).
32. A. Georges, G. Kotliar, W. Krauth, M.J. Rozenberg, Dynamical mean-field theory of strongly correlated fermion systems and the limit of infinite dimensions, Rev. Mod. Phys. 68, 13–125 (1996).
33. B.C. Zhao, Y.P. Sun, W.J. Lu, X.B. Zhu, W.H. Song, Enhanced spin fluctuations in $Ca_3Co_{4-x}Ti_xO_9$ single crystals, Phys. Rev. B 74, 144417 (2006).
34. Y.N. Huang, B.C. Zhao, J. Fang, R. Ang, Y.P. Sun, Tunning of microstructure and thermoelectric properties of $Ca_3Co_4O_9$ ceramics by high-magnetic-field sintering, J. Appl. Phys. 110, 123713 (2011).

35. Y. Wang, Y. Sui, X. Wang, W. Su, X. Liu, Enhanced high temperature thermoelectric characteristics of transition metals doped $Ca_3Co_4O_{9+\delta}$ by cold high-pressure fabrication, J. Appl. Phys. 107, 033708 (2010).
36. T. Takeuchi, T. Kondo, T. Takami, H. Takahashi, H. Ikuta, U. Mizutani, K. Soda, R. Funahashi, M. Shikano, M. Mikami, S. Tsuda, T. Yokoya, S. Shin, T. Muro, Contribution of electronic structure to the large thermoelectric power in layered cobalt oxides, Phys. Rev. B 69, 125410, 20 (2004).
37. T. Takeuchi, T. Kitao, T. Kondo, M. Mikami, Electronic structure and its contribution to the thermoelectric power of $Ca_3Co_4O_9$ and Na_xCoO_2 layered cobalt oxides, ICT2005: 24th ınternational conference on thermoelectrics (2005) pp.476–479.

Figure Captions

Figure 1. Powder X-ray diffraction patterns obtained for the $Ca_{3-x}Yb_xCo_4O_{9+\delta}$ samples; (a) x = 0.00, (b) 0.01, (c) 0.03 and (d) 0.05. The diffraction planes indicate the $Ca_3Co_4O_{9+\delta}$ phase, those indicated by a * the $Ca_3Co_2O_6$ one. The • symbol denotes the (111) plane of Si used as internal reference.

Figure 2. Surface SEM micrographs of $Ca_{3-x}Yb_xCo_4O_{9+\delta}$ samples for (a) x = 0.00, (b) 0.01, (c) 0.03 and (d) 0.05 showing the randomly oriented plate-like grains. The different contrasts have been associated to: 1) $Ca_3Co_4O_{9+\delta}$; 2) $Ca_3Co_2O_6$; and 3) Yb-rich secondary phases.

Figure 3. Temperature dependence of the resistivity of the $Ca_{3-x}Yb_xCo_4O_{9+\delta}$ samples for x= 0 (■); 0.01 (●); 0.03 (▲); and 0.05 (★).

Figure 4. $\rho(T)$ versus T^2 plots for the $Ca_{3-x}Yb_xCo_4O_{9+\delta}$ samples with x= 0 (■); 0.01 (●); 0.03 (▲); and 0.05 (★). The solid lines show the fitting curves according to equation (1).

Figure 5. ln ρ *vs*. 1/T plots according to thermally activated model for the $Ca_{3-x}Yb_xCo_4O_{9+\delta}$ samples with x= 0 (■); 0.01 (●); 0.03 (▲); and 0.05 (★). Inset shows fitting curves.

Figure 6. Temperature dependence of thermoelectric power for the $Ca_{3-x}Yb_xCo_4O_{9+\delta}$ samples with x= 0 (■); 0.01 (●); 0.03 (▲); and 0.05 (★).

Figure 7. Temperature dependence of thermal conductivity for the $Ca_{3-x}Yb_xCo_4O_{9+\delta}$ samples with x= 0 (■); 0.01 (●); 0.03 (▲); and 0.05 (★).

Figure 8. ZT as a function of temperature for the $Ca_{3-x}Yb_xCo_4O_{9+\delta}$ samples with x= 0 (■); 0.01 (●); 0.03 (▲); and 0.05 (★).

Table I. Transport properties of the $Ca_{3-x}Yb_xCo_4O_{9+\delta}$ system.

Material	T^* (K)	E_0 (meV)	$n \times 10^{21}$	E_F (eV)	ZT $\times 10^{-3}$
x=0.0	213.07	1.35	1.270	0.428	5.4
x=0.01	197.99	0.65	0.806	0.316	1.9
x=0.03	229.78	0.83	1.150	0.401	1.6
x=0.05	228.69	1.02	0.845	0.326	3.8

Figure 1

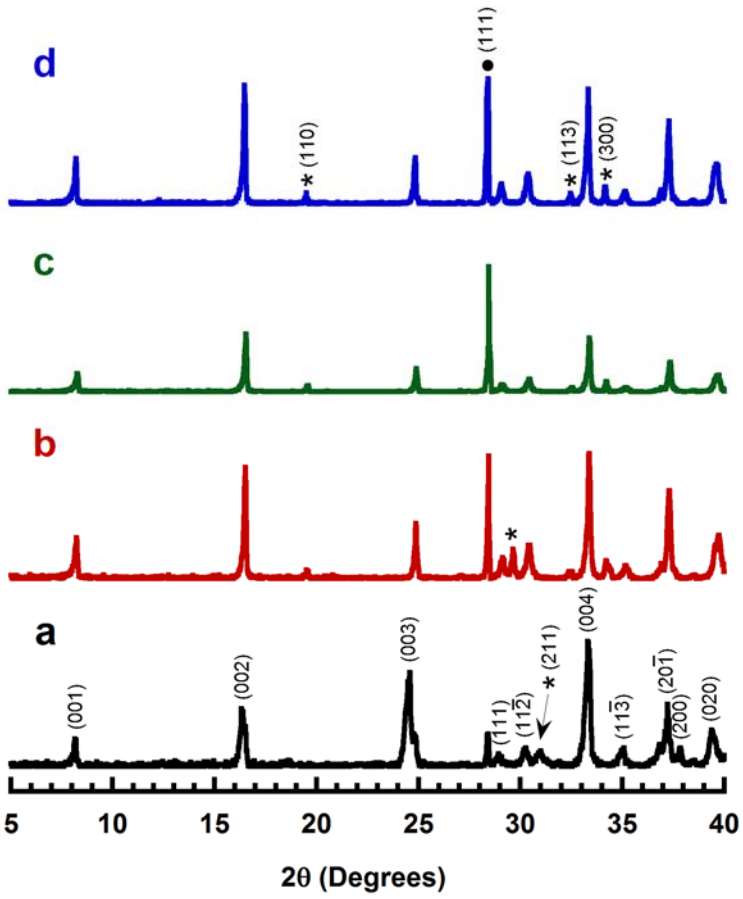
d
c
b
a
(111)
(110)
(113)
(300)
(001)
(002)
(003)
(004)
(211)
5
10
15
20
25
30
35
40
2θ (Degrees)

Figure 2

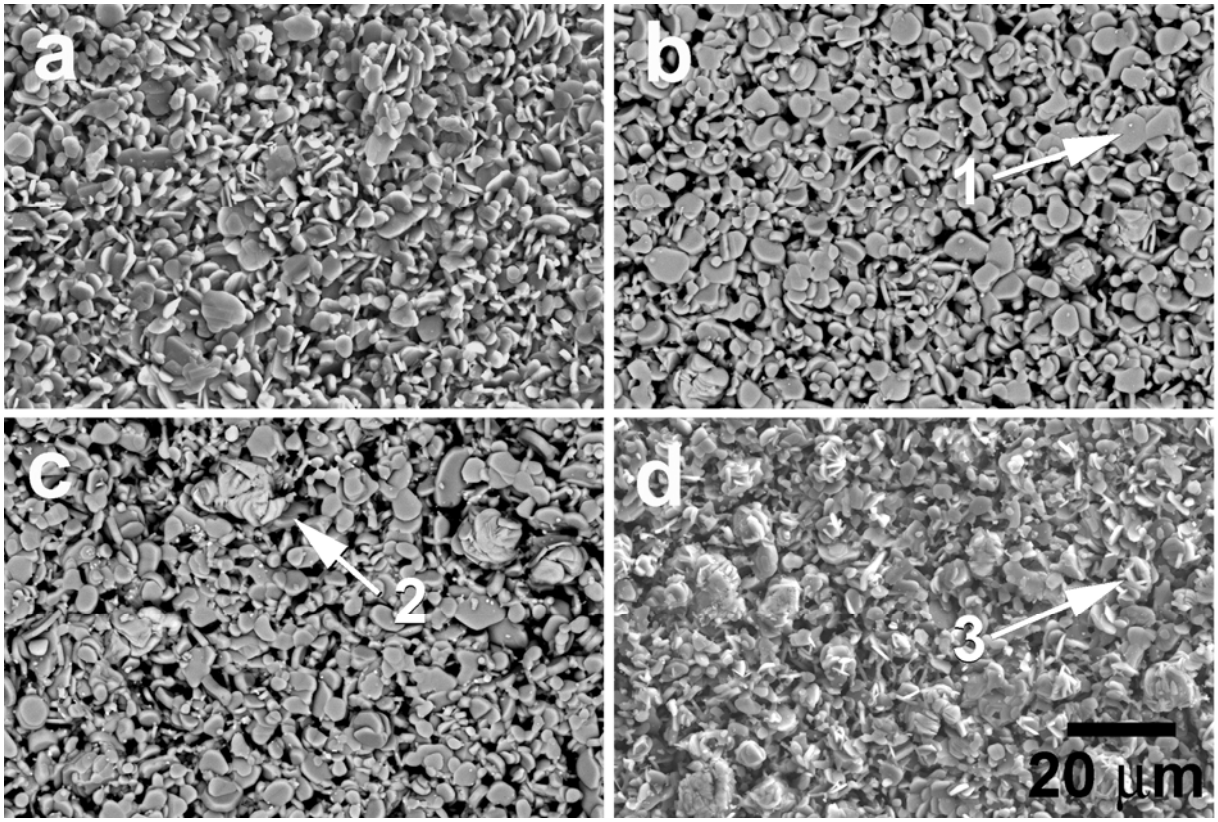

Figure 3

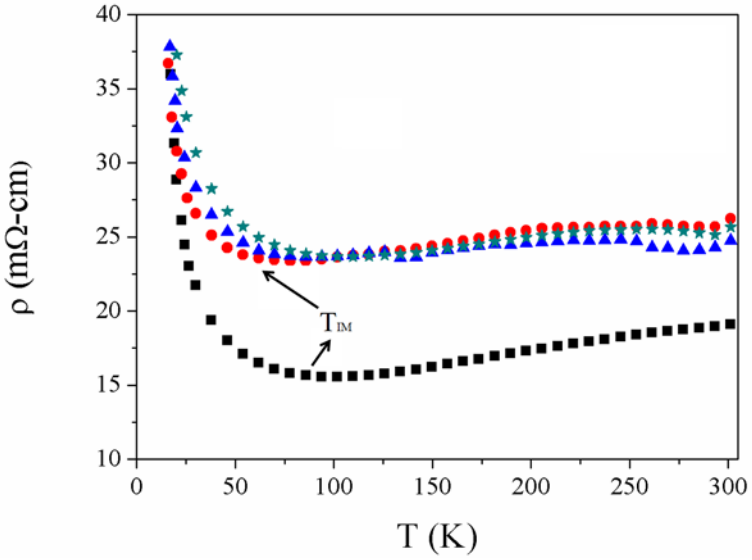

Figure 4

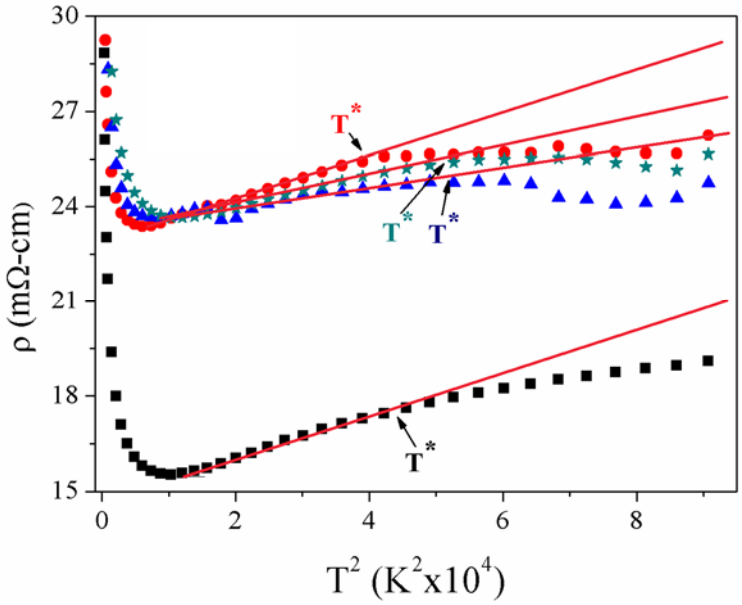

Figure 5

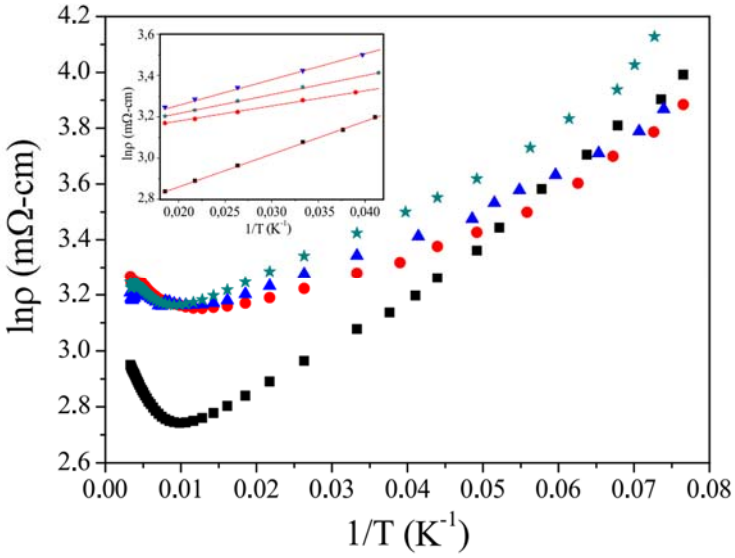
lnρ (mΩ-cm)
1/T (K-1)
4.2
4.0
3.8
3.6
3.4
3.2
3.0
2.8
2.6
0.00
0.01
0.02
0.03
0.04
0.05
0.06
0.07
0.08
3,6
3,4
3,2
3,0
2,8
0,020
0,025
0,030
0,035
0,040

Figure 6

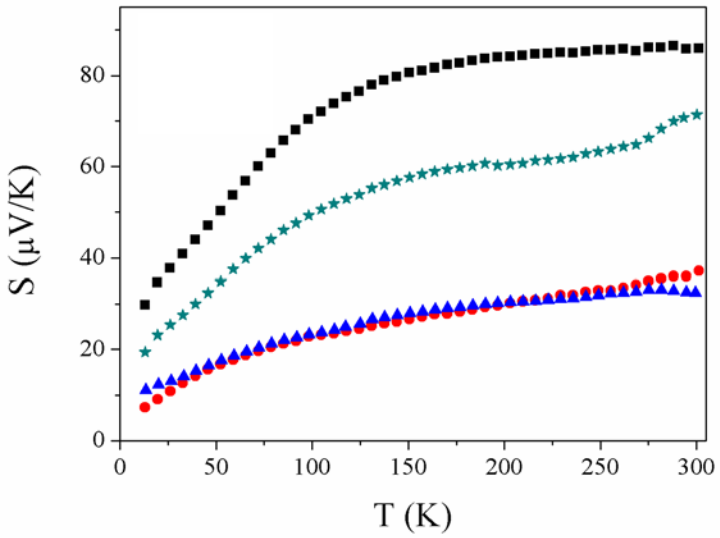

Figure 7

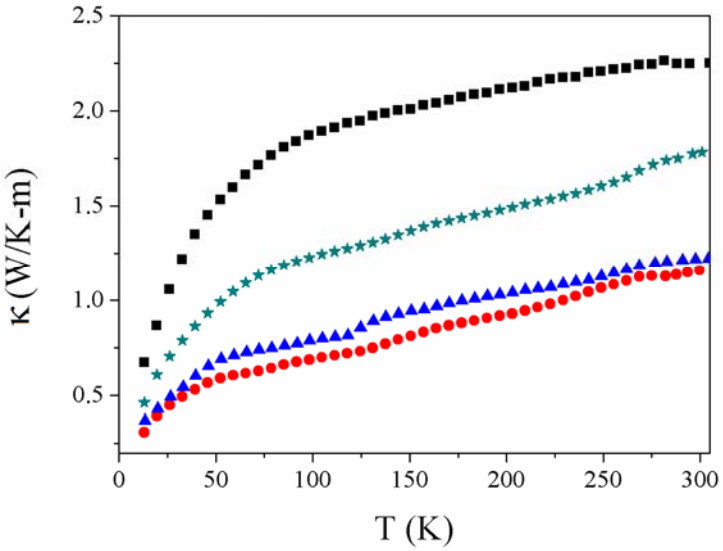

Figure 8